1999

Methanol Fuel Cell Model: Anode

S. F. Baxter

V. S. Battaglia

Ralph E. White
University of South Carolina - Columbia, white@cec.sc.edu

Publication Info

Published in *Journal of the Electrochemical Society*, Volume 146, Issue 2, 1999, pages 437-447.

Journal of The Electrochemical Society, **146** (2) 437-447 (1999)
S0013-4651(97)12-114-0 CCC: $7.00 © The Electrochemical Society, Inc.

Methanol Fuel Cell Model: Anode

S. F. Baxter,[a,*] V. S. Battaglia,[a,] and R. E. White[b,**]**

[a]*Argonne National Laboratory, Argonne, Illinois 60439, USA*
[b]*Department of Chemical Engineering, University of South Carolina, Columbia, South Carolina 29208, USA*

An isothermal, steady-state model of an anode in a direct methanol feed, polymer electrolyte fuel cell is presented. The anode is considered to be a porous electrode consisting of an electronically conducting catalyst structure that is thinly coated with an ion-selective polymer electrolyte. The pores are filled with a feed solution of 2 M methanol in water. Four species are transported in the anode: water, methanol, hydrogen ions, and carbon dioxide. All four species are allowed to transport in the x-direction through the depth of the electrode. Species movement in the pseudo y-direction is taken into account for water, methanol, and carbon dioxide by use of an effective mass-transfer coefficient. Butler–Volmer kinetics are observed for the methanol oxidation reaction. Predictions of the model have been fitted with kinetic parameters from experimental data, and a sensitivity analysis was performed to identify critical parameters affecting the anode's performance. Kinetic limitations are a dominant factor in the performance of the system. At higher currents, the polymer electrolyte's conductivity and the anode's thickness were also found to be important parameters to the prediction of a polymer electrolyte membrane fuel cell anode's behavior in the methanol oxidation region 0.5–0.6 V vs. a reversible hydrogen electrode.

Manuscript submitted December 29, 1997; revised manuscript received September 25, 1998.

Polymer electrolyte fuel cells have several characteristics that make them an attractive power source for transportation applications. In particular, they can operate on a direct feed of liquid methanol, which allows vehicle refueling to be no more labor intensive than for a spark ignition engine that runs on gasoline. A methanol/water solution is the fuel to the anode and oxygen or air to the cathode, producing the overall reaction

$$CH_3OH + 1.5\ O_2 \rightarrow CO_2 + 2H_2O \qquad [1]$$

Polymer electrolyte membrane (PEM) fuel cells operate at low temperatures, usually between 60 and 100°C, and consequently require shorter start-up times than higher temperature fuel cells. The fuel efficiency of a PEM fuel cell, fed by methanol, can be higher than an internal combustion engine because the chemical energy in methanol is directly converted to electrical energy.

The methanol feed, PEM fuel cell can be divided into seven segments (Fig. 1). The two outer segments are graphite-plate current collectors with flow channels for reactants and products to enter and exit the cell, respectively. The adjacent segments are electronically conducting porous layers that allow for even distribution of reactants to the anode and cathode. The porous layer on the anode side is a hydrophilic carbon paper while the cathode side contains a hydrophobic carbon cloth. Silicon gaskets are inserted to prevent the cell from leaking. The anode and cathode are hot-pressed onto an ion-selective polymer electrolyte membrane to construct the membrane electrode assembly (MEA) in the center of the fuel cell. Figure 2 is the expanded view of the MEA.

Figure 3 presents a schematic of the anode side of the fuel cell, which is the subject of this paper. As shown in the figure, liquid methanol and water enter through an inlet in the current collector. The reactants flow through channels that are machined into the graphite current collector. The fuel transports through an electronically conductive diffusive carbon paper. This carbon paper evenly distributes the reactants to the anode at $x = 0$. Once the water and methanol reach the anode, a series of transport processes occurs within the electrode before the following electrochemical reaction takes place (ri is used as a subscript to denote a parameter's association to a specific reaction)

$$\text{ri} = \text{I} \quad CH_3OH + H_2O \rightarrow CO_2 + 6H^+ + 6e^- \qquad [2]$$

* Electrochemical Society Student Member.
** Electrochemical Society Active Member.

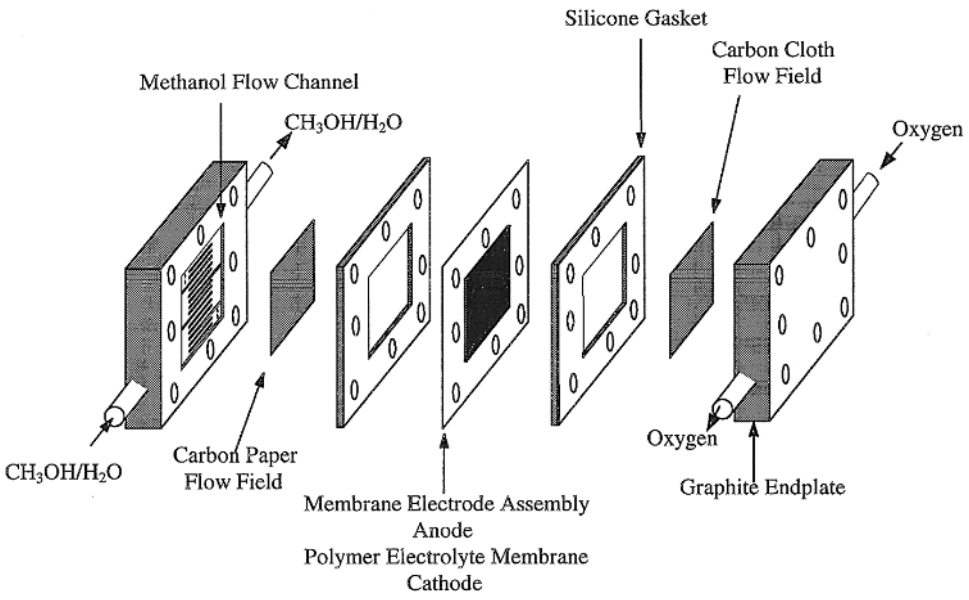

Figure 1. Schematic of a methanol feed, polymer electrolyte fuel cell.

S0013-4651(97)12-114-0 CCC: $7.00

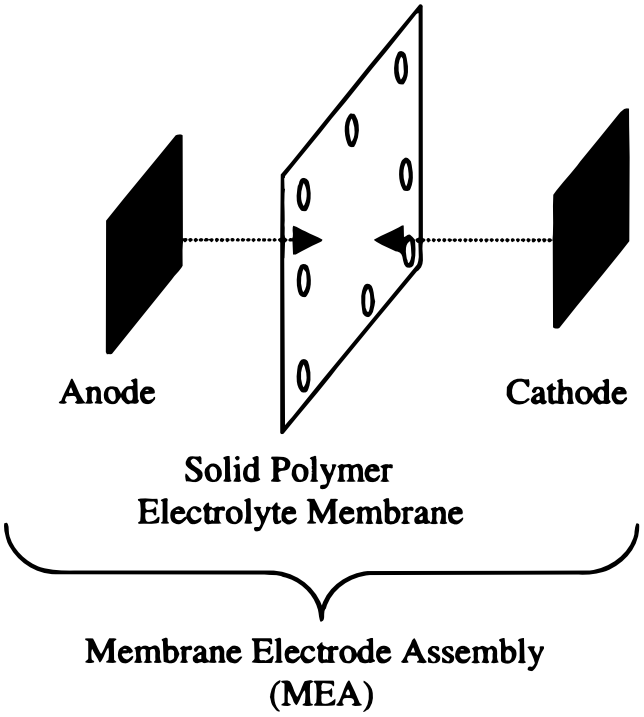

Figure 2. Schematic of a MEA shown in Fig. 1. The anode and cathode are hot-pressed onto a PEM.

The anode in Figure 3 is the type that has Nafion impregnated into the catalyst pores. Nafion impregnation means that the surface of the catalyst structure is coated with a thin layer of a solid polymer electrolyte (shaded regions between $x = 0$ and $x = L$) when Nafion is incorporated into the fabrication technique. Nafion impregnation has produced an anode with an order of magnitude less catalyst without sacrificing fuel cell performance.[1] Impregnation of solubilized Nafion in the electrode allows more of the reaction sites to be available due to the necessity of the catalyst to be in close physical contact with a hydrogen-ion-conducting electrolyte. This contact facilitates the mass transfer of hydrogen ions from the active site. The anode considered in this work is an "ink-type" electrode, and a description of its manufacturing can be found in the literature.[2,3] The porous ink electrode contains a solid matrix and a solid polymer electrolyte (referred to as the "bond layer" of the anode), with liquid feed that penetrates the pores.

As shown in Fig. 3, water and methanol transport through the carbon paper into the liquid-filled pores of the anode (unshaded regions between $x = 0$ and $x = L$). The species diffuse from the liquid pores into the polymer electrolyte bond layer. The reactants are then transported to the catalytic site where the electron-transfer reaction occurs (Eq. 2). The catalyst is a connected network of electrically active particles (known as the matrix layer) that are partially coated by an ion-selective membrane (known as the bond layer), as depicted in Fig. 4. The catalyst conducts electrons from the electrochemical reaction (Eq. 2) to an external circuit by way of the carbon paper and the current collector. The hydrogen ions that are produced in Eq. 2 remain in the bond layer. Hydrogen ions are carried through the bond layer of the anode, in the x-direction, to the proton-conducting PEM. The anodic reaction is kinetically limited, which can result in unreacted methanol and water passing through the membrane to the cathode, otherwise known as methanol crossover. Carbon dioxide, a product of the anodic reaction, will either diffuse through the membrane to the cathode or back diffuse through the carbon paper.

The two predominant issues that hinder the application of direct methanol fuel cell (DMFC) technology are poor kinetics of methanol electro-oxidation on the anode catalyst and crossover of methanol from the anode to the cathode. The effects of these two phenomena can be minimized when the anode structure promotes maximum catalyst usage and does not require methanol to be supplied in excess. In this work, the anode in a DMFC is modeled using porous electrode theory.[4] The major contribution of this work is the detailed treatment of a three-phase polymer electrolyte anode fed with a liquid methanol/water solution. A sensitivity study is presented to determine critical parameters affecting the performance of the anode.

Relevant Literature Models

Water management in the membrane has been the focus of most polymer electrolyte fuel cell models because the PEM must remain hydrated for proper fuel cell operation.[5-7] When hydrogen or a vaporized methanol/water solution is used as the fuel, hydration of the perfluorinated membrane is a serious concern. The conductivity of the membrane is directly proportional to its level of hydration. If the membrane dries out, the fuel cell cannot operate. When the fuel

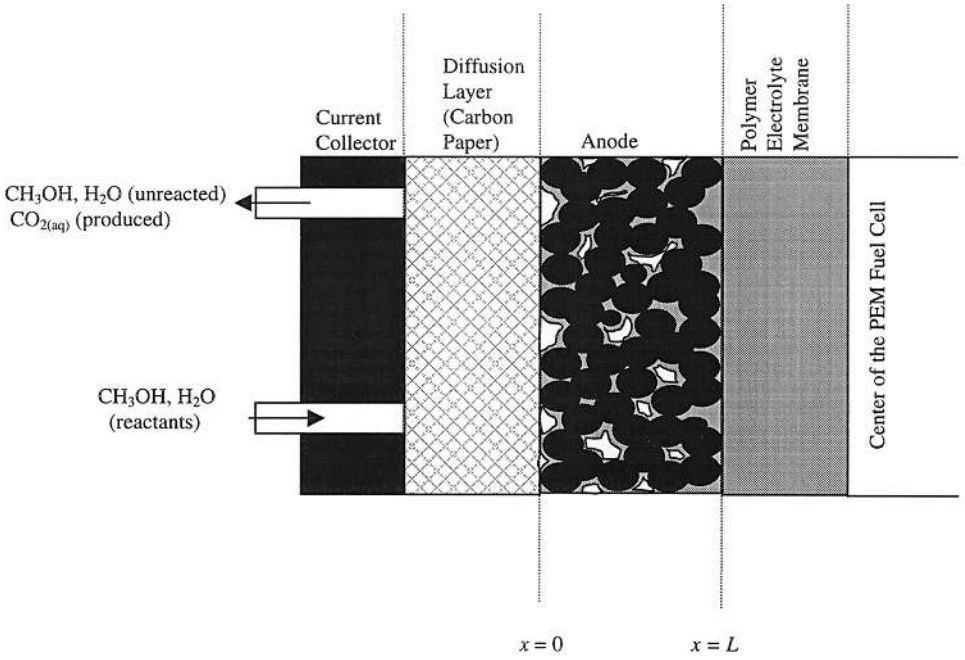

Figure 3. Schematic of the anode side of a polymer electrolyte fuel cell used in developing model.

S0013-4651(97)12-114-0 CCC: $7.00

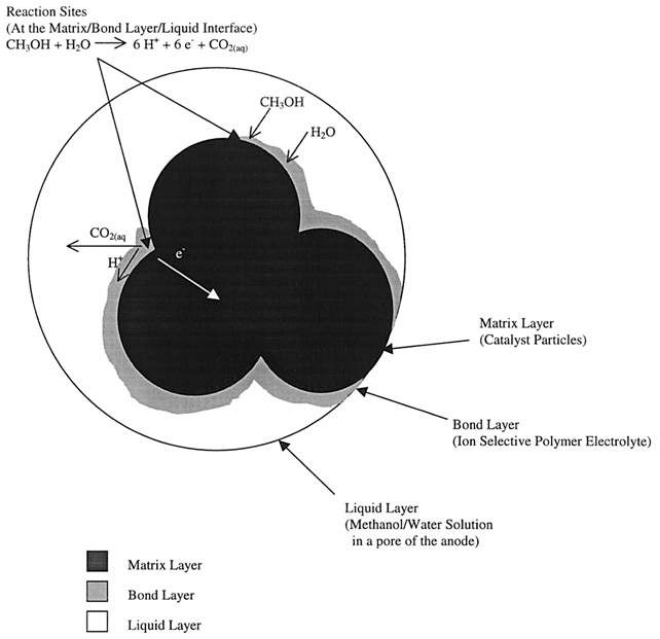

Figure 4. Exploded view of a catalyst particle (matrix layer) partially coated with polymer electrolyte (bond layer) in a porous anode. The void volume of the anode is flooded with a methanol/water solution (liquid layer).

is liquid methanol and water, our model shows that hydration of the membrane is not a problem.

Transport of methanol from the anode to the cathode results in a "chemical short" that can dramatically lower fuel cell performance. In the work presented here, methanol can transport through the membrane by diffusion and electro-osmotic drag. The diffusion coefficient of methanol in Nafion is based on Verbrugge's work. Verbrugge developed a simple diffusion-only model of methanol through a PEM, assuming dilute solution theory and no significant concentration-dependent methanol-membrane interactions.[8] After validation with experimental data, Verbrugge proved that methanol diffused through the membrane almost as readily as in a dilute solution of water. The electro-osmotic drag term for methanol is based on Fuller's concentrated solution theory model of a PEM.[9] A quantitative term for the electro-osmotic drag of water was derived from the frictional coefficient of water and hydrogen ions. The same relationship has been developed for methanol in our model.

Scott et al.[10] present a fairly simple model for a low-temperature PEM fuel cell with a vaporized methanol/oxygen feed. The purpose of this model is to determine the effect of methanol crossover on the cell voltage. The flux of water and methanol in the membrane is modeled using Fick's law and a linear concentration gradient through the thickness of the membrane. The anode in our work is more detailed kinetically and structurally. The anodic reaction is modeled with the Butler–Volmer expression rather than Tafel kinetics, which is less accurate at lower current densities. Our work treats the anode as a porous matrix coated with a polymer electrolyte that has void spaces for the liquid methanol/water solution. Scott et al. treats the pores as if they are filled with solid polymer electrolyte, eliminating any void volume for the feed to occupy. This approach requires the vaporized methanol feed to access the electrolyte from the back side of the anode (at the carbon paper/anode interface), through a fraction of the anode's geometrical area. This situation could result in membrane dehydration since the access of methanol and water through the anode is limited.

Several parameters in the model presented here are specific to the equivalent weight of the polymer electrolyte. These parameters include the drag coefficients, partition coefficients, and diffusion coefficients of water and methanol, in addition to the conductivity and thickness of the electrolyte. The equivalent weight and the molecular weight of the polymer electrolyte can be perceived as identical quantities. Using the molecular weight of the electrolyte, the concentration of sulfonic acid groups can be calculated.[9] The concentration of hydrogen ions is identical to the concentration of sulfonic acid groups due to the conservation of charge. Bernardi and Verbrugge[11] used the concentration of the electrolyte to estimate an electro-osmotic drag expression. Fuller[9] used the electrolyte concentration to determine implicitly the hydration of the membrane in order to determine a drag coefficient. The parameters (ξ_c, ξ_o, K_i, $D_{i(2)}$, κ_o, δ_m) in this work are specific to the polymer electrolyte described in this model.

Model Description

The model equations are defined in one direction (x coordinate) through the anode depth. For the movement of water, methanol, and carbon dioxide across the liquid layer/bond layer interface, a pseudo second dimension is defined in the y-direction (see Fig. 5). (Figure 5 is a simplified interpretation for the purposes of breaking down the movement of species and describing their transport in the pseudo y-

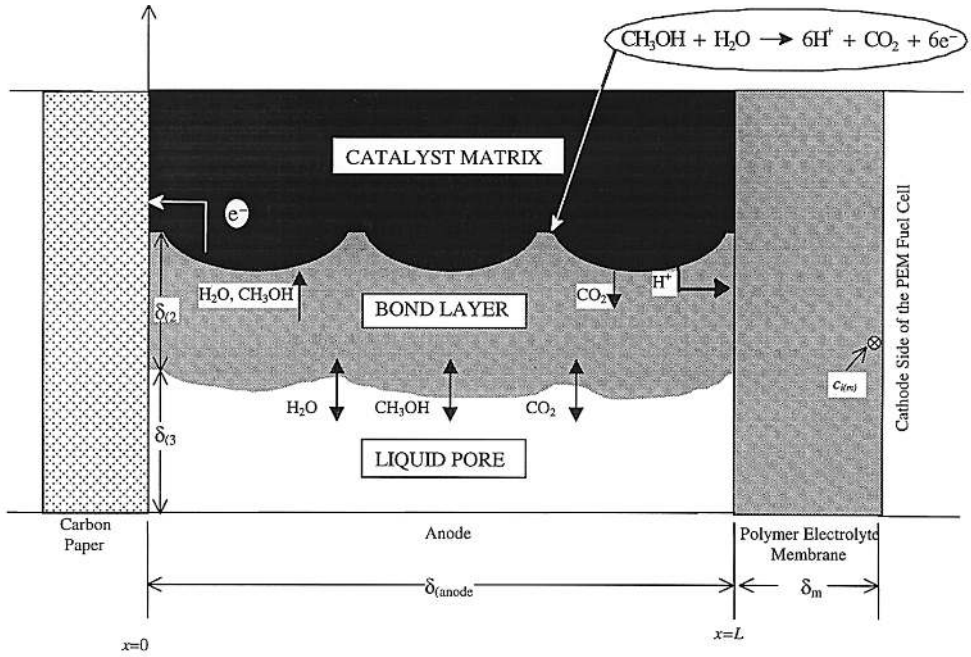

Figure 5. Schematic of the matrix, bond, and liquid layers in the anode of a PEM fuel cell. The movement of species is illustrated in the x and pseudo y directions with respect to a small volume element.

S0013-4651(97)12-114-0 CCC: $7.00

direction. It is not an actual physical representation of the anode.) Water, methanol, and carbon dioxide diffuse in the x-direction and the pseudo y-direction due to a concentration gradient. Electro-osmotic drag additionally promotes the movement of water and methanol in the x-direction. To understand the proposed movement of species previously described, it is important to realize that the layers in the model are interwoven throughout the porous electrode.

The transport of species from the liquid layer, through the bond layer, and to the catalyst surface is treated as a mass-transfer problem. The species concentration in the liquid layer is at a local x value at the center of the pore. In the bond layer the species concentration is considered to be at a local x value adjacent to the matrix surface. The concentration of species i is not accounted for through the thickness of the bond layer or the liquid layer in the y-direction. The species transports from the center of the liquid, in the pore, to the bond layer by way of diffusion in the y-direction. The concentration of species i in the bond layer, adjacent to the bond layer/liquid layer interface, is proportional to its concentration in the liquid relative to a partition coefficient, $K_i c^b_{i(3)}$. Ultimately, the bond layer species concentration, adjacent to the matrix, is related to the liquid-layer concentration at the center of the pore ($c_{i(2)}$) by an effective mass-transfer coefficient (see Appendix A). The effective mass-transfer coefficient, $k_{ri,eff}$, includes species diffusion in the liquid, transport from the liquid to the bond layer, and diffusion in the bond layer to the matrix surface. This treatment allows for the transfer of species between the anode layers. The assumptions used in this model are

1. Isothermal conditions.
2. Uniform porosity.
3. Butler–Volmer kinetics govern the electrochemical reaction.
4. The transport equations in the bond layer are based on dilute solution theory and include expressions for the electro-osmotic drag of water and methanol.
5. The transport equations in the liquid layer are based on dilute solution theory.
6. Carbon dioxide remains dissolved in solution.
7. The pressure gradient across the anode is negligible.

Applying these assumptions results in nine governing equations written for nine dependent variables with respect to the x coordinate. The dependent variables are: current density in the bond layer, i_2; electric potential in the matrix, ϕ_1; electric potential in the bond layer, ϕ_2; concentration of water in the bond layer, $c_{o(2)}$; concentration of methanol in the bond layer, $c_{c(2)}$; concentration of carbon dioxide in the bond layer, $c_{CO_2(2)}$; concentration of methanol in the liquid layer, $c_{c(3)}$; concentration of carbon dioxide in the liquid layer, $c_{CO_2(3)}$; and velocity of the liquid layer, $v_{o(3)}$.

Ohm's Law Equations

Due to the movement of charged particles, the current in the bond layer can be written[4]

$$i_2 = F\sum_i z_i N_i \quad \text{for i} = H^+ \qquad [3]$$

Hydrogen ions are the only mobile charged species in the bond layer. The flux equation for hydrogen ions in the bond layer is a function of their electrochemical potential and the electrochemical potential of water and methanol[9]

$$N_+ = -\frac{\kappa}{F}\left(\frac{\nabla\mu_+}{F} + \xi_o\frac{\nabla\mu_o}{F} + \xi_c\frac{\nabla\mu_c}{F}\right) \qquad [4]$$

In Ref. 9 an equation similar to Eq. 4 is derived for two species, water and hydrogen ions. The electro-osmotic drag (ξ_i) is defined as the ratio of the number of species i molecules (i = water or methanol) dragged by a hydrogen ion moving from one charged bond layer group to the next

$$\xi_i = \frac{N_i}{N_+} \quad \text{for } i = H_2O,\ CH_3OH \qquad [5]$$

The gradient of the electrochemical potentials can be written as[4]

$$\nabla\mu_i = RT\nabla \ln c_i + z_i F\nabla\phi_2 \qquad [6]$$

The charge numbers of water and methanol, z_i, are zero. Therefore, the electrochemical potential gradient for these two species reduces to

$$\nabla\mu_i = RT\nabla \ln c_i \quad \text{for i} = H_2O,\ CH_3OH \qquad [7]$$

The hydrogen ion concentration in the bond layer is equal to the concentration of sulfonic acid groups affixed to the Nafion electrolyte. Electroneutrality dictates that the charge of the hydrogen ions is balanced by the charged groups affixed to the Nafion backbone

$$z_+ c_{+(2)} + z_m c_m = 0 \qquad [8]$$

The concentration of sulfonic acid groups varies with the equivalent weight of polymer electrolytes. We assume that the equivalent weight of the selected polymer is uniform throughout. The charge balance in Eq. 8 states that the concentration of hydrogen ions ($c_{+(2)}$) does not vary through the electrolyte since the concentration of the sulfonic acid groups (c_m) attached to the polymer electrolyte does not vary. Therefore, $\nabla \ln c_+ = 0$, and from Eq. 6 it follows that the electrochemical potential of the hydrogen ions is only a function of the potential gradient in the bond layer

$$\nabla\mu_+ = F\nabla\phi_2 \qquad [9]$$

The equation for the ionic current (i_2) can now be written in terms of concentration and potential after substituting Eq. 4, 7, and 9 into Eq. 3

$$i_2 = -\kappa\left(\nabla\phi_2 + \xi_o\frac{RT}{F}\frac{\nabla c_{o(2)}}{c_{o(2)}} + \xi_c\frac{RT}{F}\frac{\nabla c_{c(2)}}{c_{c(2)}}\right) \qquad [10]$$

The applied total current density of the cell (I) is a known quantity. The ionic current can be calculated from Eq. 10. By conservation of charge, electronic (i_1) and ionic current densities (i_2) must sum to the total superficial current density

$$i_1 + i_2 = I \qquad [11]$$

Ohm's Law states that the electronic current in the matrix is proportional to the gradient of the potential in the x-direction. The governing equation for the potential of the matrix (ϕ_1) uses conductivity (σ) as the proportionality constant

$$i_1 = -\sigma\nabla\phi_1 \qquad [12]$$

In the model the explicit dependence on i_1 is removed by substituting Eq. 11 into Eq. 12.

Kinetic Equations

The kinetics of the methanol oxidation reaction is related to the ionic current by the Butler–Volmer expression, the governing equation for the ionic current density (i_2)

$$\frac{di_2}{dx} = a_{21} i_o\left[\exp\left(\frac{\alpha_a F}{RT}\eta_s\right) - \exp\left(\frac{-\alpha_c F}{RT}\eta_s\right)\right] \qquad [13]$$

The Butler–Volmer exchange current density can be written as a function of the reference exchange current density and the concentration of species in the liquid layer (water, methanol, and carbon dioxide)

$$i_o = i_o^\infty\left(\frac{c_{o(2)}}{c^\infty_{o(2)}}\right)^\gamma\left(\frac{c_{c(2)}}{c^\infty_{c(2)}}\right)^\pi\left(\frac{c_{CO(2)}}{c^\infty_{CO_2(2)}}\right)^\psi \qquad [14]$$

where γ, π, and ψ can be defined through a proposed reaction mechanism or fitted to experimental data. The reaction rate constants are included in the reference exchange current density (i_o^∞), measured at a given temperature and reactant concentration. The transfer current density is a function of the surface overpotential. The surface overpotential, which drives the methanol oxidation reaction (Eq. 2) at the anode, is the difference between the potential of the matrix and that of the bond layer compared to the standard potential of the reaction

S0013-4651(97)12-114-0 CCC: $7.00

$$\eta_s = \phi_1 - \phi_2 - U^{\theta}_{ref} \quad [15]$$

The reference potential is based on a platinum wire reference electrode being placed at the anode/membrane interface, adjacent to a flow of hydrogen, at 1 atm. U^{θ}_{ref} is given as

$$U^{\theta}_{ref} = U^{\theta} - \frac{1}{6F} \ln\left(\frac{c_{CO_2(2)}}{c_{o(2)}c_{c(2)}}\right) \quad (U^{\theta} = 0.029\ V \text{ vs. RHE}) \quad [16]$$

The standard potential for Eq. 2 assumes a gaseous carbon dioxide product. This model does not allow for nucleation of carbon dioxide and considers the species to be in the aqueous form.

Material Balances

Three equations (10, 12, and 13) have been presented for three dependent variables: i_1, ϕ_1, and ϕ_2. Next we present five material balance equations for five dependent variables: $c_{o(2)}$, $c_{c(2)}$, $c_{CO_2(2)}$, $c_{c(3),\text{ and }}c_{CO_2(3)}$. [Subscript (2) refers to species in the bond layer and subscript (3) refers to species in the liquid filled pores.] A ninth equation is provided to describe the velocity of liquid in the anode's pores. Three material balance equations are derived for water, methanol, and dissolved carbon dioxide species in the bond layer. Two material balances account for methanol and dissolved carbon dioxide in the liquid layer.

In the bond layer, water and methanol move in the x-direction due to diffusion and electro-osmotic drag. The flux equation describing the transport is written as

$$N_i = -\epsilon^{1.5}_{(2)} D_{i(2)} \frac{dc_{i(2)}}{dx} + \xi_i \frac{i_2}{F} \quad \text{for } i = H_2O,\ CH_3OH \quad [17]$$

Soluble carbon dioxide diffuses in the x-direction due to a concentration gradient. The carbon dioxide molecule is nonpolar and is not likely to be influenced by electro-osmotic drag. The flux of CO_2 is written as

$$N_{CO_2} = -\epsilon^{1.5}_{(2)} D_{CO_2(2)} \frac{dc_{CO_2(2)}}{dx} \quad [18]$$

At a given x location, water, methanol, and soluble carbon dioxide also move between the liquid and the bond-layer phases in a pseudo y-direction due to an assumed electrochemical potential equilibrium

$$\mu_{i(3)} = \mu_{i(2)} \quad \text{for i} = H_2O,\ CH_3OH,\ CO_2 \quad [19]$$

The transport across the bond-layer/liquid-layer interface can be described by reactions II, III, and IV (ri = I refers to Eq. 2)

$$\text{ri} = \text{II} \quad H_2O_{(3)} \rightleftharpoons H_2O_{(2)} \quad [20]$$

$$\text{ri} = \text{III} \quad CH_3OH_{(3)} \rightleftharpoons CH_3OH_{(2)} \quad [21]$$

$$\text{ri} = \text{IV} \quad CO_{2(3)} \rightleftharpoons CO_{2(2)} \quad [22]$$

The mass-transfer relationship, at operating conditions, can be described using an effective mass-transfer coefficient ($k_{ri,eff}$) and partition coefficient (K_i)

$$j_{i,eff} = k_{ri,eff}(K_i c_{i(3)} - c_{i(2)}) \quad \text{for i} = H_2O,\ CH_3OH,\ CO_2 \quad [23]$$

The concentration $c_{i(3)}$ is the concentration of species i at the center of the pore in the liquid layer. The concentration $c_{i(2)}$ is the concentration of species i in the bond layer (at the matrix surface). These concentrations vary only in the x-direction of a given layer. The effective flux of species i, $j_{i,eff}$, has no dependence on the x coordinate at a local concentration position. The effective flux defined in Eq. 23 describes the rate of mass transfer from the liquid layer to the matrix surface using a pseudo y coordinate. The derivation of Eq. 23 can be found in Appendix A. Mass-transfer contributions in the pseudo y-direction are important for the transport of species to and from the catalyst reaction site.

Once the electrochemical reaction occurs at the matrix/bond-layer interface, water and methanol are consumed while carbon dioxide is formed at a rate given by the equation

$$j_i = \frac{-s_{i,1}}{6F}\frac{di_2}{dx} \quad \text{for i} = H_2O,\ CH_3OH,\ CO_2 \quad [24]$$

where $s_{i,I}$ is the stoichiometric coefficient of species i in the electrochemical reaction of Eq. 2 (denoted by the subscript I). Equations 17, 23, and 24 can be combined to yield the material-balance equations for water and methanol in the bond layer

$$\frac{d}{dx}\left(\epsilon^{1.5}_{(2)} D_{i(2)} \frac{dc_{i(2)}}{dx} - \xi_i \frac{i_2}{F}\right) = -a_{23}k_{ri,eff}(K_i c_{i(3)} - c_{i(2)}) - \frac{s_{i,ri}}{nF}\frac{di_2}{dx} \quad [25]$$

Equations 18, 23, and 24 can be combined to give the carbon dioxide mole balance in the bond layer

$$\frac{d}{dx}\left(\epsilon^{1.5}_{(2)} D_{CO_2(2)} \frac{dc_{CO_2(2)}}{dx}\right) = -a_{23}k_{IV,eff}(K_{CO_2}c_{CO_2(3)} - c_{CO_2(2)}) - \frac{s_{CO_2,I}}{nF}\frac{di_2}{dx} \quad [26]$$

The left side of Eq. 25 and 26 represents the difference between the flux entering and exiting the volume element in the x-direction. The first term on the right side of Eq. 25 and 26 quantifies the flux across the bond-layer/liquid-layer interface in the pseudo y-direction. The second term on the right side of Eq. 25 and 26 is a generation (or consumption) term for the species involved in the electrochemical reaction.

Two additional material balances describe the movement of methanol and carbon dioxide in the liquid layer. The liquid phase is modeled using dilute solution theory. Here the solvent is water, and the solutes are methanol and dissolved carbon dioxide. The flux of both solute species is composed of diffusion and convection components. In addition, both species exchange across the bond-layer/liquid-layer interface in the pseudo y-direction, as described previously. The material balances for methanol and carbon dioxide are Eq. 27 and 28, respectively

$$\frac{d}{dx}\left(\epsilon^{1.5}_{(3)} D_{c(3)} \frac{dc_{c(3)}}{dx} - c_{c(3)}v_{o(3)}\right) = a_{23}k_{III}(K_c c_{c(3)} - c_{c(2)}) \quad [27]$$

$$\frac{d}{dx}\left(\epsilon^{1.5}_{(3)} D_{CO_2(3)} \frac{dc_{CO_2(3)}}{dx} - c_{CO_2(3)}v_{o(3)}\right) = a_{23}k_{IV}(K_{CO_2}c_{CO_2(3)} - c_{CO_2(2)}) \quad [28]$$

The convection term in Eq. 27 and 28 is based on the solvent velocity in the liquid layer. The water's velocity can be equal to the bulk velocity of the liquid layer, since water is considered to be the solvent. The flux of water in the liquid layer is equal to the product of its concentration and velocity. Since the concentration of water does not change significantly, the velocity of water can be written as

$$\frac{dv_{o(3)}}{dx} = \frac{dN_{o(3)}/dx}{c_{o(3)}} = \frac{a_{23}k_{II}(K_o c_{o(3)} - c_{o(2)})}{c_{o(3)}} \quad [29]$$

Governing Equations and Boundary Conditions

The nine independent equations for the nine dependent variables are listed with each equation's appropriate boundary conditions.

Matrix Layer

1. Ohm's law for dependent variable ϕ_1

$$0 \le x < L \quad i_1 = -\sigma\frac{d\phi_1}{dx} \quad [30]$$

$$\text{at } x = L \quad i_1 = 0 \quad [31]$$

S0013-4651(97)12-114-0 CCC: $7.00

At the electrode/membrane interface, $x = L$, the superficial current is purely ionic, carried by the positively charged hydrogen ions.

Bond Layer

2. Modified Ohm's law for dependent variable ϕ_2

$0 \leq x < L$

$$i_2 = -\kappa\left(\frac{d\phi_2}{dx} + \xi_o \frac{RT}{Fc_{o(2)}}\frac{dc_{o(2)}}{dx} + \xi_c \frac{RT}{Fc_{c(2)}}\frac{dc_{c(2)}}{dx}\right) \quad [32]$$

$$\text{at } x = L \quad \phi_2 = 0 \quad [33]$$

Assuming a reference electrode is present at $x = L$, the potential of the bond layer is set to zero at the interface.

3. Butler–Volmer kinetic expression for dependent variable i_2

$$0 < x \leq L \quad \frac{di_2}{dx} = a_{21} i_o \left[\exp\left(\frac{\alpha_a F}{RT}\eta_s\right) - \exp\left(\frac{-\alpha_a F}{RT}\eta_s\right)\right] \quad [34]$$

$$\text{at } x = 0 \quad i_2 = 0 \quad [35]$$

4. Flux balance of water, in the bond layer, for dependent variable $c_{o(2)}$

$0 < x < L$

$$\frac{d}{dx}\left(\epsilon_{(2)}^{1.5} D_{o(2)} \frac{dc_{o(2)}}{dx} c_{o(2)} - \xi_o \frac{i_2}{F}\right) = -a_{23} k_{II,eff}(K_o c_{o(3)} - c_{o(2)}) - \frac{s_{o,II}}{nF}\frac{di_2}{dx} \quad [36]$$

$$\text{at } x = 0 \quad N_{o(2)} = 0 \quad [37]$$

at $x = L$

$$N_{o(2)} = -D_{o(2)}\frac{(c_{o(m)} - c_{o(2)})}{\delta_m} + \xi_o \frac{i_2}{F} - c_{o(3)} v_{o(3)} \quad [38]$$

where δ_m is the thickness of the membrane, and $c_{o(m)}$ is a set concentration of water at the membrane/cathode interface.

5. Flux balance of methanol, in the bond layer, for dependent variable $c_{c(2)}$

$$0 < x < L \quad \frac{d}{dx}\left(\epsilon_{(2)}^{1.5} D_{c(2)} \frac{dc_{c(2)}}{dx} - \xi_c \frac{i_2}{F}\right) = -a_{23} k_{III,eff}(K_c c_{c(3)} - c_{c(2)}) - \frac{s_{c,III}}{nF}\frac{di_2}{dx} \quad [39]$$

$$\text{at } x = 0 \quad N_{c(2)} = 0 \quad [40]$$

$$\text{at } x = L \quad N_{c(2)} = -D_{c(2)}\frac{(c_{c(m)} - c_{c(2)})}{\delta_m} + \xi_c \frac{i_2}{F} - N_{c(3)} \quad [41]$$

where $c_{c(m)}$ is a set concentration at the membrane/cathode interface and $N_{c(3)}$ is defined in Eq. 47.

6. Flux balance of carbon dioxide, in the bond layer, for dependent variable $c_{CO_2(2)}$

$$0 < x < L \quad \frac{d}{dx}\left(\epsilon_{(2)}^{1.5} D_{CO_2(2)} \frac{dc_{CO_2(2)}}{dx}\right) = -a_{23} k_{IV,eff}(K_{CO_2} c_{CO_2(3)} - c_{CO_2(2)}) - \frac{s_{CO_2,I}}{nF}\frac{di_2}{dx} \quad [42]$$

$$\text{at } x = 0 \quad N_{CO_2(2)} = 0 \quad [43]$$

at $x = L$

$$N_{CO_2(2)} = -\frac{D_{CO_2(2)}}{\delta_m} c_{CO_2(2)}\left(\frac{D_{CO_2(2)}/\delta_m}{k'_{IVc} + D_{CO_2(2)}/\delta_m} - 1\right) - N_{CO_2(3)} \quad [44]$$

where $N_{CO_2(3)}$ is defined in Eq. 50.

The flux of species into the bond layer (at $x = 0$) from the feed stream is a negligible quantity compared to the higher flux of species from the liquid layer into the bond layer. This is due to the high specific surface area of the bond layer in contact with the liquid layer compared to the geometric surface area of the bond layer in contact with the feed stream. The difference between these fluxes could be minimized or reversed if significant carbon dioxide evolution caused the volume fraction shared by the liquid and vapor to become predominantly or wholly occupied by vapor.

The exiting flux from the bond layer (at $x = L$) is based on diffusion coefficients of species in the membrane and the concentration gradient across the membrane. The membrane and bond layer consist of the same material, and it is assumed that the same diffusion coefficient applies in both regions. In addition, methanol and water have an added influence of electro-osmotic drag from the anode to the cathode side of the membrane. The concentrations of methanol and water are assumed to be fixed at the membrane/cathode interface. Since methanol that crosses through the membrane preferentially reacts at the cathode, the concentration at the membrane/cathode interface is set to zero. The concentration of water on the cathode side of the membrane is considered high enough to maintain membrane saturation. The flux of carbon dioxide exiting the bond layer is based on transport relationships across the membrane and cathode regions. These relationships permit the concentration of carbon dioxide in the cathode effluent to be set to a value. The equation for the exiting flux of carbon dioxide is developed in Appendix B.

Liquid Layer

7. Flux balance of methanol, in the liquid layer, for dependent variable $c_{c(3)}$

$0 < x < L$

$$\frac{d}{dx}\left(\epsilon_{(3)}^{1.5} D_{c(3)} \frac{dc_{c(3)}}{dx} - c_{c(3)} v_{o(3)}\right) = a_{23} k_{III,eff}(K_c c_{c(3)} - c_{c(2)}) \quad [45]$$

$$\text{at } x = 0 \quad c_{c(3)} = c_c^o \quad [46]$$

$$\text{at } x = L \quad N_{c(3)} = \epsilon_{(3)} k_{III}(K_c c_{c(3)} - c_{c(2)}) \quad [47]$$

8. Flux balance of carbon dioxide in the liquid layer for dependent variable $c_{CO_2(3)}$

$$0 < x < L \quad \frac{d}{dx}\left(\epsilon_{(3)}^{1.5} D_{CO_2(3)} \frac{dc_{CO_2(3)}}{dx} - c_{CO_2} v_{o(3)}\right) = a_{23} k_{IV,eff}(K_{CO_2} c_{CO_2(3)} - c_{CO_2(2)}) \quad [48]$$

$$\text{at } x = 0 \quad c_{CO_2(3)} = 0 \quad [49]$$

$$\text{at } x = L \quad N_{CO_2(3)} = \epsilon_{(3)} k_{IV}(K_{CO_2} c_{CO_2(3)} - c_{CO_2(2)}) \quad [50]$$

In the liquid layer the inlet concentrations of methanol and dissolved carbon dioxide are set by the feed stream composition to the anode.

The rate of methanol and dissolved carbon dioxide flux into the polymer electrolyte membrane from the liquid layer (at $x = L$) is dependent on a mass-transfer coefficient. Because the bond layer and membrane are the same polymer electrolyte material, the concentration of species i at the membrane side of the liquid-layer/membrane interface is the same as the concentration of species i on the bond-layer side of the bond-layer/membrane interface ($c_{i(2)}$).

9. Velocity of water

$$0 \leq x < L \quad \frac{dv_{o(3)}}{dx} = \frac{dN_{o(3)}/dx}{c_{o(3)}} = \frac{ak_{II}(K_o c_{o(3)} - c_{o(2)})}{c_{o(3)}} \quad [51]$$

$$\text{at } x = L \quad v_{o(3)} = \frac{N_{o(3)}}{c_{o(3)}} = \frac{\epsilon_{(3)} k_{II}(K_o c_{o(3)} - c_{o(2)})}{c_{o(3)}} \quad [52]$$

The velocity of water at the liquid-phase/membrane interface is set equal to the flux of water at $x = L$, divided by its concentration.

S0013-4651(97)12-114-0 CCC: $7.00

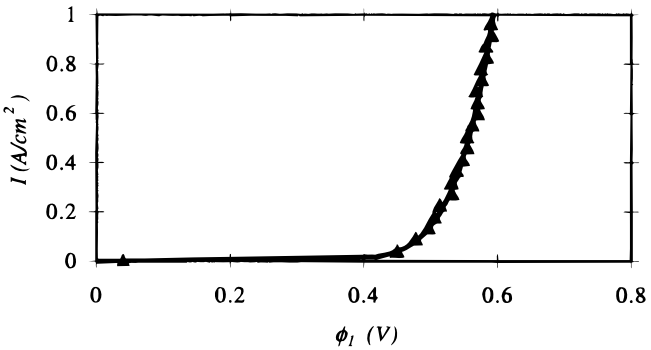

Figure 6. Polarization curve of methanol oxidation on a PtRu catalyst (90:10 mol %). Cell conditions are 2 M methanol feed vs. hydrogen, 0/0 atm, 70°C, Pt/C cathode: (▲) experimental data vs. (—) the model prediction. Electrode area is 5 cm^2.

Sensitivity Analysis

A sensitivity analysis was used to determine the model parameters that most influence the performance of the anode. The method used in this paper is patterned after a study done by Kimble and White.[12] The model was first fitted with kinetic parameters from experimental data that indicate the anodic performance of a methanol-fed, polymer-electrolyte fuel cell (Fig. 6). The experimental data were obtained from a methanol-fed, polymer-electrolyte fuel cell operated with a hydrogen-producing cathode. (In an operational fuel cell, water is produced by the oxygen reduction reaction on the cathode.) The cathode was treated as a reversible hydrogen electrode (RHE) by supplying it with hydrogen gas at 1 atm. In this manner the cathode polarization is minimized. Based on a full DMFC model to be presented in a future paper, results indicate that the anode will remain hydrated with a 2 M methanol feed. Full-fuel-cell model predictions suggest that the anode of a methanol/hydrogen fuel cell will perform similarly to the anode of a methanol/oxygen fuel cell. The experimental data obtained from the described methanol/hydrogen fuel cell were corrected to reflect the potential drop in the anode. The potential loss across the membrane is subtracted using an Ohm's law relationship. The remaining potential losses in the data are attributed to the anode. The model prediction fits the data to a standard deviation of approximately 9 mV. In Fig. 6 the most active range for anodic methanol oxidation is between 0.5 and 0.6 V vs. RHE. Our data are consistent with previously determined potential regions for methanol oxidation on a platinum–ruthenium catalyst surface.[13-15] Currents closely corresponding to this operating range, 0.1–1.0 A/cm^2, were used as the sensitivity limits. The parameter values in the model, used to fit the data, are considered the "base-case" parameter values.

To determine a sensitivity coefficient, each base-case parameter value was singularly increased 5% while all other parameters were held at their base-case values. The resultant cell potential and increased parameter value were combined as follows to determine the sensitivity coefficients in units of volts

$$\frac{\partial \phi_l}{\partial \ln \theta_j} = \frac{\phi_l - \phi_l^*}{\dfrac{\theta_j - \theta_j^*}{\theta_j^*}} \qquad [53]$$

where θ_j is the 5% increased parameter value, ϕ_l is the resultant potential, θ_j^* is the base-case parameter value, and symbol ϕ_l^* is the predicted cell potential when all the base-case parameters are employed. The tested parameters and their base-case values are listed in Table I. The model is most sensitive to variations in the anode thickness, the bond layer's conductivity, the anodic transfer coefficient, and the product of the exchange current density and specific surface area associated with the methanol oxidation reaction. Positive values of the sensitivity coefficient indicate higher polarization.

The sensitivity of the model predictions to the conductivity of the bond layer can be explained using the sensitivity curve generated in Fig. 7. Sensitivity coefficients are calculated using the higher intrinsic conductivity of the bond layer ($\kappa_o = 1.05\ \kappa_o^*$) plotted over the corresponding operating range of currents. This curve suggests that the model prediction is more sensitive to the conductivity of the bond layer at higher current densities, because the sensitivity curve deviates more strongly from zero at increased currents. This is explained by the fact that kinetic polarization becomes less of a factor than ohmic resistance at higher currents.

Figure 8 illustrates the varying effects associated with increasing the anode's thickness. [The base-case thickness was measured by scanning electron microscopy (SEM).] Increasing the thickness of the anode affects its performance in two conflicting ways. The area for exchange of current between the bond layer and the matrix increases (ai_o). This effectively reduces the local current density and therefore, the local polarization. Increasing the distance through which the current must flow results in an additional potential drop across the electrode. Additional ohmic drop results in a more positive value of the sensitivity coefficient at higher currents. Thicker anodes not only have large ohmic potential drops at higher currents but also result in a poorly used electrode and wasted catalyst.

The model predictions are most sensitive to the kinetic parameters in the Butler–Volmer expression. The base-case values for these parameters were fitted to the experimental data in Fig. 6. The

Table I. Base-case parameter values.

Parameter	Value	Units
Specific surface area ($a_{21}i_o$)	4.5×10^{-5}	A/cm^3
Specific surface area (a_{23})	1300	cm^{-1}
Anode thickness (δ_a)	1.00×10^{-3}	cm
Electro-osmotic drag coefficient of H_2O (ξ_o)	2.5	
Electro-osmotic drag coefficient of CH_3OH (ξ_c)	2.48×10^{-2}	
Mass-transfer coefficient of H_2O ($k_{II,eff}$)	1.00×10^{-3}	cm/s
Mass-transfer coefficient of CH_3OH ($k_{III,eff}$)	2.28×10^{-4}	cm/s
Mass-transfer coefficient of CO_2 ($k_{IV,eff}$)	6.13×10^{-2}	cm/s
Partition coefficient of H_2O (K_o)	1.0	
Partition coefficient of CH_3OH (K_c)	0.8	
Partition coefficient of CO_2 (K_{CO2})	6.3	
Conductivity of bond layer (κ)	2.0×10^{-2}	S/cm
Effective conductivity of matrix (σ)	8.13×10^{6}	S/cm
Concentration of H_2O in feed ($c_{o(3)}$ at $x = 0$)	5.54×10^{-2}	mol/cm^3
Concentration of CH_3OH in feed ($c_{c(3)}$ at $x = 0$)	2.0×10^{-2}	mol/cm^3
Temperature (T)	343	K
Anodic transfer coefficient (α_a)	0.8	

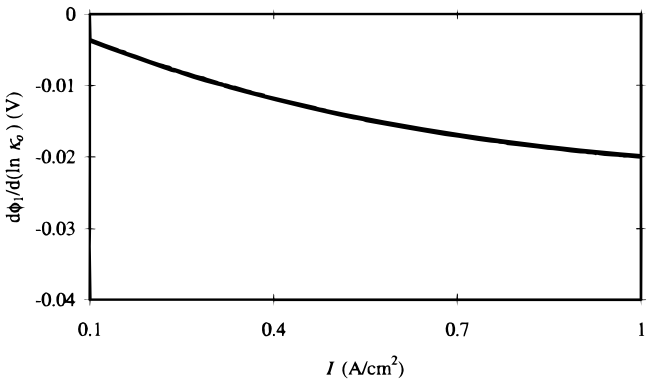

Figure 7. Sensitivity of the model predictions to the conductivity of the bond layer.

S0013-4651(97)12-114-0 CCC: $7.00

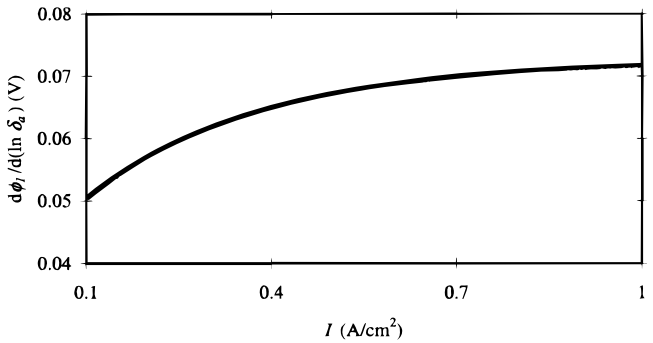

Figure 8. Sensitivity of the model predictions to anode thickness.

curves in Fig. 9 and 10 indicate that increasing the kinetic parameters results in negative sensitivity curves indicative of a lower ohmic drop across the anode. In Fig. 9 the ai_o term (the product of the exchange current density and the matrix-to-bond layer specific surface area) has been increased 5%, and the sensitivity curve indicates a decrease in potential uniformly through the entire current range. The sensitivity curve is nearly flat because the transfer current into the matrix is mostly uniform throughout the anode for all current densities. This is due to the already large kinetic polarization.

Figure 10 shows the sensitivity of the potential drop to the anodic transfer coefficient of the Butler–Volmer expression. The model prediction is almost an order of magnitude more sensitive to the anodic transfer coefficient than to any other model-sensitive parameter. This is due to the exponential dependence of the Butler–Volmer expression on α_a (in all cases, $\alpha_a + \alpha_c = 6$).

The sensitivity analysis was used to determine which parameters need to be measured most accurately to yield a valid prediction of the anode's polarization. The model predictions varied negligibly for the other parameters in Table II when increased 5%. The model is very sensitive to variations in temperature. The temperature analysis is not provided here due to an incomplete set of parameter values at different temperatures. This sensitivity indicates that it is important to evaluate correctly model-sensitive parameters at the operating temperature. Overall, the sensitivity analysis shows that the electrode performance is more limited by reaction polarization than mass-transfer limitations, especially in the range of 0.5–0.6 V vs. the hydrogen reference electrode. It should be noted that the electrode simulated in this study was not optimized but was merely a case study of a working anode with direct methanol feed in a PEMFC.

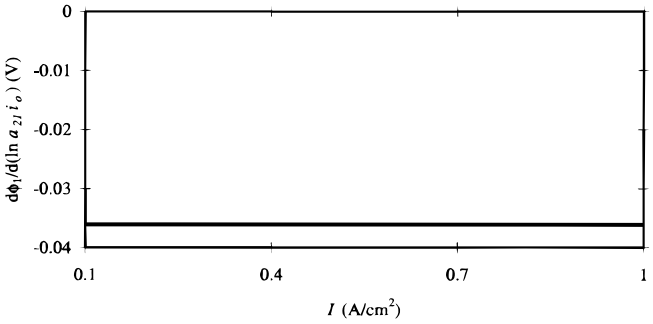

Figure 9. Sensitivity of the model predictions to the product of the exchange current density and the matrix-to-bond layer specific surface area of methanol electro-oxidation on PtRu catalyst.

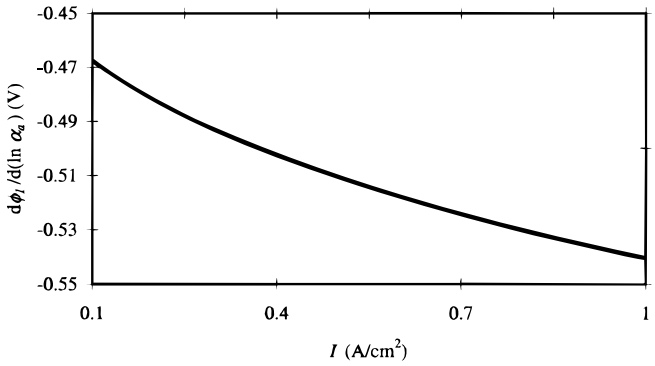

Figure 10. Sensitivity of the model predictions to the anodic transfer coefficient of methanol electro-oxidation on PtRu catalyst.

Additional Results from Model Predictions

As mentioned previously, the loss of cell voltage due to the crossover of methanol from the anode to the cathode is a critical issue to the advancement of methanol-fed, polymer-electrolyte fuel cells. The following model predictions were obtained for the previously described anode in a fuel cell operated at 0.5 A/cm^2. In Fig. 11 the concentration of methanol in the liquid layer is shown to decrease by approximately 0.01 M across the thickness of the anode. The concentration of methanol in the bond layer (Fig. 12) decreases slightly due to Eq. 2 but is still at a very high percentage of its inlet concentration (for $x > 0$, $c^o_{c(2)} = c^o_{c(3)}K_c$). The methanol is supplied in such excess that a 1.99 M solution is available in the liquid layer and a nearly 1.37 M concentration in the bond layer at the anode/membrane interface ($x = L$). To predict the methanol crossover, we use the model-predicted methanol concentrations adjacent to the membrane and assume any methanol contacting the cathode is immediately burned or electrochemically consumed in a working PEMFC. At an applied current of 0.5 A/cm^2, the electrode described in this paper has a ratio of 0.8 for the flux of methanol (due to diffusion and electro-osmotic drag) to the flux of protons across the membrane. These calculations are based on a PEMFC with the same material transport properties in the bond layer as the membrane.

Table II. Parameter values.

Parameter	Value	Units
a_{23}	1300	cm^{-1}
$c_{o(m)}$	$c_{o(3)}K_o$	mol/cm^3
$c_{c(m)}$	0.0	
$c^\infty_{o(2)}$	0.554	mol/cm^3
$c^\infty_{c(2)}$	0.02	mol/cm^3
$c^\infty_{CO2(2)}$	1×10^{-4}	mol/cm^3
$D_{o(2)}$	7.3×10^{-6} exp[2436(1/353 − 1/T)], Ref. 10	cm^2/s
$D_{c(2)}$	4.9×10^{-6} exp[2436(1/333 − 1/T)], Ref. 10	cm2/s
$D_{CO2(2)}$	1×10^{-7}	cm^2/s
$D_{c(3)}$	1.6×10^{-5}, Ref. 8	cm^2/s
$D_{CO2(3)}$	1×10^{-6}	cm^2/s
K_o	1.0	
K_c	0.8, Ref. 17	
K_{CO2}	6.3	
$k_{II,eff}$	1.0×10^{-3}	cm/s
$k_{III,eff}$	2.74×10^{24} exp(−22187.5/T), Ref. 18	cm/s
$k_{IV,eff}$	6.13×10^{-2}	cm/s
T	343.15	K
U^θ	0.029	V
α_a	0.8	
α_c	5.2	
γ	0.08	
π	0.08	
ψ	0.92	
δ_a	1.0×10^{-3}	cm
δ_m	0.02	cm
$\epsilon_{(1)}$	0.26	
$\epsilon_{(2)}$	0.27	
$\epsilon_{(3)}$	0.47	
κ_o	0.01, Ref. 19	S/cm
σ	8.13×10^6, Ref. 20	S/cm
ξ_o	2.5	
ξ_c	2.48×10^{-2}, Ref. 10	

S0013-4651(97)12-114-0 CCC: $7.00

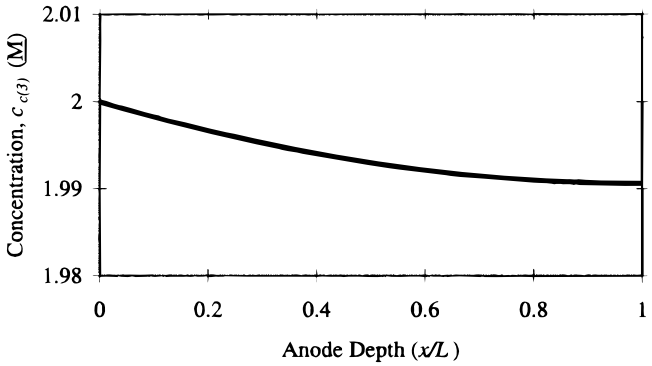

Figure 11. Concentration profile of methanol through the liquid layer. The applied current is 0.5 A/cm^2.

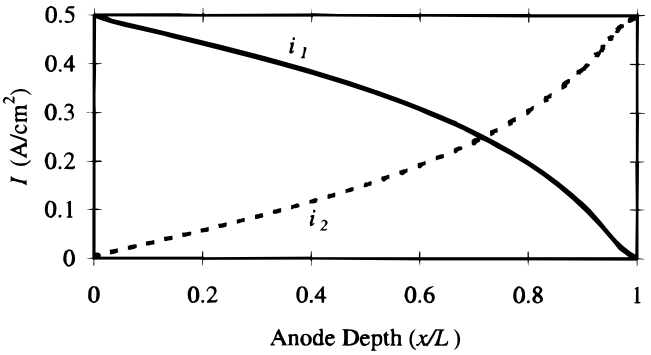

Figure 13. Current distribution through the thickness of a porous PEMFC anode. The electronic current is i_1, and the ionic current is i_2. The applied current is 0.5 A/cm^2.

The production of carbon dioxide gas within the anode can cause a loss of anodic performance. Trapped gas in the anode's pores limits its access of liquid fuel to the catalyst and renders the sites inactive. With enough gas evolution, the hydration of the bond layer decreases, and the ohmic drop across the anode increases significantly. The model can be used to calculate the fuel flow rate needed to sweep carbon dioxide away from the face of the anode at a rate fast enough to keep the carbon dioxide concentration within the pores and bond layer below the gas solubility limit. At 70°C, the solubility limit for carbon dioxide in the liquid layer is 1.4×10^{-5} mol/cm^3. [16] The model demonstrates that if the carbon dioxide concentration at the anode face is kept below 9.0×10^{-6} mol/cm^3, the liquid volume's carbon dioxide concentration does not exceed the solubility limit at currents as high as 1 A/cm^2. The fuel volumetric flow rate can then be calculated using the flux of the methanol/water solution at the face of the anode, the carbon dioxide concentration, and the geometrical surface area of the electrode. For a 5 cm^2 anode, a fuel flow rate of 37 cm^3/min is needed to prevent carbon dioxide gassing at 1 A/cm^2.

In a porous electrode, the current is transferred from the matrix to the bond layer, and the sum of the two is always equal to a constant (see Eq. 11). An even transfer of current from the matrix to the electrolyte through the depth of the electrode indicates that the reaction rate is uniform, and that the electrode is being fully used for the oxidation of methanol. Figure 13 shows the reaction distribution is fairly uniform through the electrode. Such a distribution typically signifies an electrode that is kinetically limited. At lower applied currents the reaction would be even more uniform. This overall analysis points to a need for higher-surface-area catalysts.

Conclusions

In this work the transport of water, methanol, carbon dioxide, and hydrogen ions through a porous anode has been characterized. The porous anode was impregnated with a PEM and contained a certain void volume to allow access of methanol and water through the depth of the electrode. The results of this model show that the kinetics of methanol oxidation and the active specific surface area are the primary limiting factors given the parameters associated with PtRu catalysts. The model can also predict the amount of methanol crossover through the membrane at given current densities and the necessary fuel flow rate to maintain water-soluble levels of carbon dioxide in the anode's liquid-filled pores.

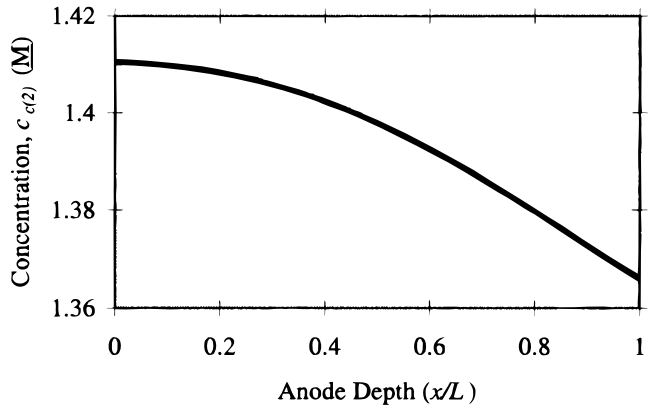

Figure 12. Concentration profile of methanol through the bond layer. The applied current is 0.5 A/cm^2.

Acknowledgments

The authors thank Dr. Romesh Kumar and Dr. Deborah Myers, Argonne National Laboratory, for their technical assistance and Dr. Anthony Aldykiewicz, W. R. Grace, who performed the methanol/hydrogen experiment. This work was supported by the Army Research Office and the U.S. Department of Energy.

The University of South Carolina assisted in meeting the publication costs of this article.

Appendix A

The concentration of species i in the liquid layer can be related to its concentration at the matrix surface by deriving a flux equation in the pseudo y-direction. The dependent-variable concentrations in the liquid layer ($c_{o(3)}$, $c_{c(3)}$, $c_{CO_2(3)}$) are values at the center of a pore in the anode. The dependent-variable concentrations in the bond layer ($c_{o(2)}$, $c_{c(2)}$, $c_{CO_2(2)}$) are values in the bond layer/matrix interface where the electrochemical reaction occurs. The transport of a species from the liquid to the matrix can be divided into three segments. The first component of the flux is the diffusion of species i from the center of the pore to a position that is within the liquid layer, adjacent to the liquid-layer/bond-layer interface, approximated as

$$j_{i(3)} = \frac{D_{i(3)}}{\delta_{(3)}/2}(c_{i(3)} - c^{b}_{i(3)}) \quad \text{for i} = H_2O, CH_3OH, CO_2 \qquad [A\text{-}1]$$

where $j_{i(3)}$ is the flux of species i in the liquid layer; $D_{i(3)}$ is the diffusion coefficient of species i in the liquid; $\delta_{(3)}$ is the thickness of the liquid layer; $c_{i(3)}$ is the average concentration of species i in the center of the liquid volume element; and $c^{b}_{i(3)}$ is the concentration of species i within the liquid-layer, adjacent to the liquid-layer/bond-layer interface.

The second component is the equilibrium condition that is assumed to exist across the liquid-layer/bond-layer interface by the relationships

$$H_2O_{(3)} \rightleftharpoons H_2O_{(2)} \qquad [A\text{-}2]$$

$$CH_3OH_{(3)} \rightleftharpoons CH_3OH_{(2)} \qquad [A\text{-}3]$$

$$CO_{2(3)} \rightleftharpoons CO_{2(2)} \qquad [A\text{-}4]$$

The concentration of species i on the bond-layer side of the interface can be related to the concentration on the liquid layer side of the interface with a partition coefficient

$$c^{b}_{i(2)} = K_i c^{b}_{i(3)} \quad \text{for i} = H_2O, CH_3OH, CO_2 \qquad [A\text{-}5]$$

where K_i is the partition coefficient of species i at the bond-layer/liquid-layer interface and $c^{b}_{i(2)}$ is the concentration of species i within the bond-layer, adjacent to the liquid-layer/bond-layer interface.

The third component is the diffusion of species i across the bond-layer to the matrix surface

S0013-4651(97)12-114-0 CCC: $7.00

$$j_{i(2)} = \frac{D_{i(2)}}{\delta_{(2)}}(c^{b}_{i(2)} - c_{i(2)}) \quad \text{for i} = H_2O, CH_3OH, CO_2 \qquad [A\text{-}6]$$

where $D_{i(2)}$ is the diffusion coefficient of species i in the bond layer, $\delta_{(2)}$ is the thickness of the bond layer, and $c_{i(2)}$ is the bond-layer concentration of species i at the surface of the matrix.

Substituting Eq. A-5 into Eq. A-6 yields

$$j_{i(2)} = \frac{D_{i(2)}}{\delta_{(2)}}(K_i c^{b}_{i(3)} - c_{i(2)}) \qquad [A\text{-}7]$$

Solving Eq. A-1 for $c^{b}_{i(3)}$ yields

$$c^{b}_{i(3)} = -j_{i(3)}\frac{\delta_{(3)}/2}{D_{i(3)}} + c_{i(3)} \qquad [A\text{-}8]$$

Substituting Eq. A-8 into A-7 yields a *y*-direction flux equation

$$j_{i(2)} = \frac{D_{i(2)}}{\delta_{(2)}}\left(K_i\left(-j_{i(3)}\frac{\delta_{(3)}/2}{D_{i(3)}} + c_{i(3)}\right) - c_{i(2)}\right) \qquad [A\text{-}9]$$

The equation for the *y*-direction flux is a function of the concentration of species i in the liquid layer, $c_{i(3)}$, and the concentration of species i at the matrix surface, $c_{i(2)}$.

At steady state, the flux in the *y*-direction is a constant and equal to an effective *y*-direction flux

$$j_{i(3)} = j_{i(2)} = j_{i,eff} \qquad [A\text{-}10]$$

Rearranging Eq. A-9 and substituting Eq. A-10 for the *j* terms yields

$$j_{i,eff}\left(K_i\frac{\delta_{(3)}/2}{D_{i(3)}} + \frac{\delta_{(2)}}{D_{i(2)}}\right) = (K_i c_{i(3)} - c_{i(2)}) \qquad [A\text{-}11]$$

An effective mass-transfer coefficient can now be defined for movement in the *y*-direction

$$\frac{1}{k_{ri,eff}} = \left(K_i\frac{\delta_{(3)}/2}{D_{i(3)}} + \frac{\delta_{(2)}}{D_{i(2)}}\right) \qquad [A\text{-}12]$$

Substituting Eq. A-12 into Eq. A-11 yields the flux equation for species in the pseudo *y*-direction (Eq. 23) in terms of $c_{i(2)}$ and $c_{i(3)}$

$$j_{i,eff} = k_{ri,eff}(K_i c_{i(3)} - c_{i(2)}) \quad \text{for i} = H_2O, CH_3OH, CO_2 \qquad [A\text{-}13]$$

Appendix B

In the bond layer the boundary condition for species at $x = L$ depends on the concentration of the species at the membrane/cathode interface. The concentration of methanol at the cathode is set to zero because it is assumed that the methanol is immediately oxidized upon reaching the cathode. The concentration of water is set to the membrane saturation value. The concentration of carbon dioxide is not set at the membrane/cathode interface but at the cathode/gas inlet interface. The boundary condition eliminates the concentration of carbon dioxide at the cathode from the exiting bond-layer flux equation.

The total flux of carbon dioxide across the membrane is a function of the concentration gradient across the membrane and the diffusion coefficient of carbon dioxide in the membrane

$$N_{CO_2(m)} = -D_{CO_2(2)}\frac{(c_{CO_2(m)} - c_{CO_2(2)})}{\delta_m} \qquad [B\text{-}1]$$

(See Fig. 5 for the location of $c_{i(m)}$). The same diffusion coefficient for carbon dioxide in the bond layer can be used in this equation since the bond layer and the membrane are the same ion-selective, polymer membrane material.

The flux of carbon dioxide across the membrane is equal to the flux of carbon dioxide out of the cathode

$$N_{CO_2(m)} = N_{CO_2(cathode)} = -a_{cathode}\delta_{cathode}k_{IVc}(K'_{CO_2}c_{CO_2(cathode)} - c_{CO_2(m)}) \qquad [B\text{-}2]$$

Setting Eq. B-1 equal to Eq. B-2 and solving for the concentration of carbon dioxide in the membrane yields

$$c_{CO_2(m)} = \frac{a_{cathode}\delta_{cathode}k_{IVc}K'_{CO_2}c_{CO_2(cathode)} + c_{CO_2}D_{CO_2(2)}/\delta_m}{a_{cathode}\delta_{cathode}k_{IVc} + D_{CO_2(2)}/\delta_m} \qquad [B\text{-}3]$$

Substituting Eq. B-3 into Eq. B-1 yields the flux across the membrane, with no dependence on the membrane's concentration of carbon dioxide

$$N_{CO_2(2)} = -\frac{D_{CO_2(2)}}{\delta_m}\left(\frac{a_{cathode}\delta_{cathode}k_{IVc}K'_{CO_2}c_{CO_2(cathode)}}{a_{cathode}\delta_{cathode}k_{IVc} + D_{CO_2(2)}/\delta_m} + \frac{c_{CO_2}D_{CO_2(2)}/\delta_m}{a_{cathode}\delta_{cathode}k_{IVc} + D_{CO_2(2)}/\delta_m} - c_{CO_2(2)}\right) \qquad [B\text{-}4]$$

The concentration of carbon dioxide in the cathode effluent is much less than the concentration of carbon dioxide in the membrane or bond layer of the anode. Equation B-4 reduces to Eq. 44

$$N_{CO_2(m)} = -\frac{D_{CO_2(2)}}{\delta_m}c_{CO_2(2)}\left(\frac{D_{CO_2(2)}/\delta_m}{k'_{IVc} + D_{CO_2(2)}/\delta_m} - 1\right) \qquad [B\text{-}5]$$

where

$$k'_{IVc} = a_{cathode}\delta_{cathode}k_{IVc} \qquad [B\text{-}6]$$

List of Symbols

a_{21}	specific surface area of the anode's bond layer in contact with matrix, cm^{-1}
a_{23}	specific surface area of the anode's bond layer in contact with liquid, cm^{-1}
$a_{cathode}$	specific surface area of the cathode's bond layer in contact with matrix, cm^{-1}
$c_{o(l)}$	concentration of water per unit volume in phase l(l = 2, bond layer; l = 3, liquid), mol/cm^3
$c_{c(l)}$	concentration of methanol per unit volume in phase l, mol/cm^3
$c_{CO_2(l)}$	concentration of carbon dioxide (aq) per unit volume in phase l, mol/cm^3
$c_{CO_2(cathode)}$	concentration of carbon dioxide (aq) per unit volume in the cathode, mol/cm^3
$c_{i(m)}$	concentration of species i at the membrane/cathode interface, mol/cm^3
$c^{\infty}_{i(2)}$	reference concentration of species i for the reference exchange current density (i^{∞}_o), mol/cm^3
$c^{b}_{i(2)}$	concentration of species i in the liquid layer, adjacent to the bond layer, mol/cm^3
$c^{b}_{i(3)}$	concentration of species i in the bond layer, adjacent to the liquid layer, mol/cm^3
$D_{o(2)}$	actual diffusion coefficient of water in the bond layer phase, cm^2/s
$D_{c(l)}$	actual diffusion coefficient of methanol in phase l, cm^2/s
$D_{CO_2(l)}$	actual diffusion coefficient of carbon dioxide (aq) in phase l, cm^2/s
F	Faraday's constant, 96,487 C/equiv
I	superficial current density to an electrode, A/cm^2
i_1	superficial current density in the matrix, A/cm^2
i_2	superficial current density in the bond layer, A/cm^2
i_o	exchange current density for Eq. 2, A/cm^2
i^{∞}_o	exchange current density for Eq. 2 at known reference conditions, A/cm^2
j_i	flux of species i in the x-direction, $mol/cm^2/s$
$j_{i(l)}$	flux of species i in the y-direction of layer l, $mol/cm^2/s$
$j_{i,eff}$	effective flux of species i in the y-direction, $mol/cm^2/s$
K_i	partition coefficient of species i
K'_{CO_2}	partition coefficient of carbon dioxide in the cathode
k_{ri}	mass-transfer coefficient of equilibrium condition ri, cm/s
k_{IVc}	mass-transfer coefficient of the carbon dioxide (aq) equilibrium condition in the cathode, cm/s
k'_{IVc}	mass-transfer coefficient defined by Eq. B-6, cm/s
$k_{ri,eff}$	effective y-direction mass-transfer coefficient of equilibrium condition, ri, cm/s
L	thickness of the anode, cm
$N_{i(l)}$	flux of species i in phase l, $mol/cm^2/s$
$N_{i(m)}$	flux of species i across the membrane, $mol/cm^2/s$
R	gas constant, 8.314 3 J/mol/K
$s_{i,I}$	stoichiometric coefficient of species i in anodic Eq. 2
$s_{i,ri}$	stoichiometric coefficient of species i in equilibrium condition, ri
T	temperature, K
U^{θ}	standard potential of Eq. 2 (0.029 V vs. RHE)
$v_{o(3)}$	velocity in the liquid layer, cm/s
x	local position coordinate in the anode
z_+	charge on a hydrogen ion (+1)
z_m	charge on a sulfonic ion group (−1)

S0013-4651(97)12-114-0 CCC: $7.00

Greek

α_a	anodic transfer coefficient
α_c	cathodic transfer coefficient
γ, π, ψ	exponents in composition dependence on the exchange current density
δ_a	anode thickness, cm
$\delta_{cathode}$	cathode thickness, cm
δ_m	membrane thickness, cm
$\delta_{(l)}$	thickness of layer *l*, cm
$\epsilon_{(l)}$	fraction of total electrode volume occupied by phase *l*
ϕ_1	electric potential in the matrix, V
ϕ_1^*	electric potential in the matrix after a 5% increase of a base-case parameter, V
ϕ_2	electric potential in the bond layer, V
η_s	surface overpotential, V
κ	effective conductivity of the bond layer, $\kappa = \kappa_o \epsilon_{(2)}^{1.5}$, S/cm
κ_o	conductivity of the polymer electrolyte outside of a porous structure, S/cm
μ_i	electrochemical potential of species i, J/mol
θ_j^*	base-case parameter value used in sensitivity analysis
θ_j	parameter that has been increased 5% for sensitivity analysis ($\theta_j = 1.05\theta_j^*$)
σ	effective conductivity of the solid matrix, S/cm
ξ_o	electro-osmotic coefficient of water (ξ_o = flux of water/flux of hydrogen ions)
ξ_c	electro-osmotic coefficient of methanol (ξ_c = flux of methanol/flux of hydrogen ions)

Subscripts

c	methanol (CH_3OH)
CO_2	carbon dioxide (CO_2)
l	$l = 1$, matrix layer; $l = 2$, bond layer; $l = 3$, liquid layer
m	electrolyte's sulfonic acid group
ri	refers to reaction I, II, III, or IV
	I. $CH_3OH + H_2O \rightarrow 6H^+ + CO_2 + 6e^-$ (anodic reaction)
	II. $H_2O_{(3)} \rightleftharpoons H_2O_{(2)}$ (equilibrium condition in the anode)
	III. $CH_3OH_{(3)} \rightleftharpoons CH_3OH_{(2)}$ (equilibrium condition in the anode)
	IV. $CO_{2(3)} \rightleftharpoons CO_{2(2)}$ (equilibrium condition in the anode)
o	water (H_2O)
+	hydrogen ion (H^+)
1	matrix phase
2	bond-layer phase
3	liquid phase

References

1. G. G. Scherer, *Solid State Ionics,* **94,** 249 (1997).
2. M. S. Wilson and S. Gottesfeld, *J. Appl. Electrochem.,* **22,** 1 (1992).
3. X. Ren, M. S. Wilson, and S. Gottesfeld, *J. Electrochem. Soc.,* **143,** L12 (1996).
4. J. S. Newman, *Electrochemical Systems,* 2nd ed., Prentice Hall, Englewood Cliffs, NJ (1991).
5. D. M. Bernardi, *J. Electrochem. Soc.,* **137,** 3344 (1990).
6. T. F. Fuller and J. Newman, *J. Electrochem. Soc.,* **140,** 1218 (1993).
7. T. V. Nguyen and R. E. White, *J. Electrochem. Soc.,* **140,** 2178 (1993).
8. M. W. Verbrugge, *J. Electrochem. Soc.,* **136,** 417 (1989).
9. T. F. Fuller, Thesis, University of California, Berkeley, CA (1992).
10. K. Scott, W. Tamma, and J. Cruickshank, *J. Power Sources,* **65,** 159 (1997).
11. D. M. Bernardi and M. W. Verbrugge, *J. Electrochem. Soc.,* **139,** 2477 (1992).
12. M. C. Kimble and R. E. White, *J. Electrochem. Soc,* **139,** 478 (1992).
13. A. Aramata and W. Veerasai, *Electrochim. Acta,* **36,** 1043 (1991).
14. P. S. Kauranen, E. Skou, and J. Munk, *J. Electroanal. Chem.,* **404,** 1 (1996).
15. N. M. Markovic, H. A. Gasteiger, P. N. Ross, Jr., X. Jiang, I. Villegas, and M. J. Weaver, *Electrochim. Acta,* **40,** 91 (1995).
16. *Perry's Chemical Engineers' Handbook,* 50th ed., R. H. Perry and D. Green, Editors, McGraw-Hill, Inc., New York (1984).
17. P. S. Kauranen, Thesis, Helsinki University of Technology, Finland (1996).
18. J. Cruickshank and K. Scott, *J. Power Sources,* **70,** 40 (1998).
19. T. E. Springer, M. S. Wilson, and S. Gottesfeld, *J. Electrochem. Soc.,* **140,** 3513 (1993).
20. *Handbook of Chemistry and Physics,* 74th ed., D. R. Lide, Editor, CRC Press, Boca Raton, FL (1983).